HHS Public Access

Author manuscript

Biomaterials. Author manuscript; available in PMC 2018 March 30.

Published in final edited form as:

Biomaterials. 2015 January ; 39: 164–172. doi:10.1016/j.biomaterials.2014.10.078.

Lithography-Free Fabrication of Reconfigurable Substrate Topography For Contact Guidance

Pitirat Pholpabu[a], **Stephen Kustra**[a], **Haosheng Wu**[b], **Aditya Balasubramanian**[b], and **Christopher J. Bettinger**[a,b]

[a]Department of Biomedical Engineering, Carnegie Mellon University, 5000 Forbes Avenue, Pittsburgh, PA 15213, USA

[b]Department of Materials Science and Engineering, Carnegie Mellon University, 5000 Forbes Avenue, Pittsburgh, PA 15213, USA

Abstract

Mammalian cells detect and respond to topographical cues presented in natural and synthetic biomaterials both in vivo and in vitro. Micro- and nano-structures influence the adhesion, morphology, proliferation, migration, and differentiation of many phenotypes. Although the mechanisms that underpin cell-topography interactions remain elusive, synthetic substrates with well-defined micro- and nano-structures are important tools to elucidate the origin of these responses. Substrates with reconfigurable topography are desirable because programmable cues can be harmonized with dynamic cellular responses. Here we present a lithography-free fabrication technique that can reversibly present topographical cues using an actuation mechanism that minimizes the confounding effects of applied stimuli. This method utilizes strain-induced buckling instabilities in bi-layer substrate materials with rigid uniform silicon oxide membranes that are thermally deposited on elastomeric substrates. The resulting surfaces are capable of reversible of substrates between three distinct states: flat substrates (A = 1.53 ± 0.55 nm, Rms = 0.317 ± 0.048 nm); parallel wavy grating arrays ($A_{||}$ = 483.6 ± 7.8 nm and $\lambda_{||}$ = 4.78 ± 0.16 μm); perpendicular wavy grating arrays ($A_{\perp}$ = 429.3 ± 5.8 nm; $\lambda_{\perp}$ = 4.95 ± 0.36 μm). The cytoskeleton dynamics of 3T3 fibroblasts in response to these surfaces was measured using optical microscopy. Fibroblasts cultured on dynamic substrates that are switched from flat to topographic features (FLAT-WAVY) exhibit a robust and rapid change in gross morphology as measured by a reduction in circularity from 0.30 ± 0.13 to 0.15 ± 0.08 after 5 min. Conversely, dynamic substrate sequences of FLAT-WAVY-FLAT do not significantly alter the gross steady-state morphology. Taken together, substrates that present topographic structures reversibly can elucidate dynamic aspects of cell-topography interactions.

Keywords

topography; contact guidance; microfabrication; microstructure

Introduction

Mammalian cells can detect the topography of biomaterials in both natural and synthetic microenvironments [1–5]. Topography plays an important role in determining the collective cell behavior in many complex biological processes in development, wound healing, and tissue regeneration [1,4,6–11]. Topographical cues control fundamental cellular functions including adhesion, migration, proliferation, and differentiation [12–16]. Most phenomenological studies that correlate cell function with feature geometry and size employ substrates with static structures [7,17–25]. Static surfaces can extract many complex mechanisms that underpin cell-materials interactions such as contact guidance. However, there is a limit to the insight that can be gained by interrogating dynamic systems with static cues. Substrates that present topography with spatiotemporal control are advantageous in studying cell-materials interactions including contact guidance. They can potentially decouple contact guidance responses from other confounding processes such as cell attachment and spreading [5,26].

Controlled presentation of topographical cues has improved through recent advances in stimuli-responsive materials [27,28] precise delivery of stimuli such as temperature changes, light, or mechanical strain [1,4,10,16,20,28,29]. This strategy has been used for dynamic microstructure presentation to study cell-materials interactions in numerous contexts [1,3,5,30]. Programmable topography can also be engineered using stimuli-responsive polymers including those that respond to cues such as electric fields, temperature changes, and enzymes [3,5,27,31,32].

The introduction of external stimuli may affect baseline metabolism, viability, or proliferation of cell populations [33]. For example, changes in temperature, the presence of enzymes, or irradiated light can impact basal cell function [3,33]. Mechanical stimuli via direct application of strain is advantageous for topographic feature formation because it is rapid, robust, and facile [1,5]. Most currently available methods that use strain-induced topography require uniaxial strains of greater than 10% [1,26,34]. Mammalian cells can detect strains of the underlying substrate as small as 3.5% and respond to these stains by altering their morphology [35,36]. Therefore, inducing topographic features using mechanical strains >3.5% may convolve contact guidance with responses to substrate deformation. Strain-induced topography will ideally utilize mechanical stimuli that are below the lower limit of detection for mammalian cells. Furthermore, mechanical stimuli can be coupled with materials that can reversibly present homogeneous topographical cues in various orientations. Herein we report a lithography-free fabrication technique that is capable of producing strain-induced topography using sub-threshold uniaxial strains. Cytoskeleton morphodynamics in fibroblasts are measured using these model surfaces.

Materials & Methods

Fabrication and Characterization of Programmable Dynamic Topography

Elastomeric substrates were prepared using polydimethylsiloxane (PDMS, Sylgard 184, Dow Corning, Midland, MI USA) cured in a 10:1 ratio at 75 °C. Rectangular PDMS coupons (W x L x H = 1.5 cm x 3.5 cm x 600 μm) were mounted in a custom fixation device

and strained to the desired amount. Pre-strained substrates were coated with 100 nm of silicon oxide (SiO_x) deposited by thermal evaporation. Briefly, silicon monoxide (SiO) was thermally deposited at a rate of 1 Å/sec at 10^{-6} Torr (NexDep, Angstrom Engineering, Kitchener, ON Canada). All substrates were processed in an identical manner with the exception that the thickness of the bi-layer membrane was set at either 10 or 100 nm. Dynamic topography sequences were switched between states in less than 3 sec. Microstructures of bilayer membranes were characterized using optical microscopy (Olympus BH2 microscope, Olympus America Inc., Center Valley, PA USA) and atomic force microscopy (AFM, Dimension 3100 SPM, Veeco, Plainville, NY USA). Fourier transforms of optical micrographs were prepared using ImageJ (National Institute of Health, USA, available at http://rsb.info.nih.gov/ij).

Fibroblast Culture and Imaging

All cell culture supplies were purchased from Invitrogen (Carlsbad, CA USA) unless otherwise stated. Bi-layer membranes were sterilized in ethanol (70% v/v) and irradiated with UV for 30 min. Bi-layer membranes were incubated with RGD solution (50 μg/cm^2) for 40 min and rinsed with 3x PBS. NIH 3T3 fibroblasts (ATCC, Monassas, VA USA) were seeded at densities of 25,000 cells/cm^2 and incubated in DMEM medium supplemented with 10% fetal bovine serum (FBS) and 1% penicillin/streptomycin (P/S) at 37 °C. Live cell images were performed by culturing cells for 24 hr prior to dynamic topography sequences. Cells were cultured in en environmentally controlled chamber set at 37 °C with >90% relative humidity and 5% CO_2 (BioImager, Mississauga, ON Canada). FB were imaged in phase contrast and analyzed using NIH ImageJ to measure morphology and relative orientation. Cell circularity was calculated using the following expression.

$$C_{cell} = \frac{4\pi A_{proj}}{P^2} \quad \text{Eqn. 1}$$

where A_{proj} and P are the projected surface area and perimeter of the cell, respectively. The axial ratio R_{axis} was calculated from the length of the major axis divided by the length of the minor axis (Figure S1) [37].

Cells were fixed in 4% formaldehyde for 20 min, stained using 20 μL of Alexa Fluor® 488 Phalloidin (200 U/mL), and counterstained with SlowFade® Gold Antifade Reagent with DAPI. Phase contrast and fluorescent images were recorded using an EvosFL microscope (Advanced Microscopy Group, Bothell, WA USA). FB on a static substrate were also imaged using confocal fluorescence microscopy (LSM 510 META DuoScan, Carl Zeiss, Heidelberg Germany) and scanning electron microscopy (SEM) (PhilipsXL-30 FEG, FEI, Hillsboro, OR, USA). Cells dedicated for SEM imaging were fixed in 4% formaldehyde for 20 min, washed with distilled water for 3 times, and dehydrated in a series of mixtures containing ethanol and hexamethyldisilazane (HDMS), as previously described [38]. Dehydrated samples were coated with 4 nm of platinum prior to imaging (Emtech K575X, Quorum Technologies, Guelph, ON, Canada).

Statistical Methods

Cell morphodynamic measurements were based on at least 100 cells per each data point and all experiments were repeated in triplicate. All data is shown as mean ± s. e. m. unless otherwise stated. A student's t-test with p-value of 0.05 was performed to consider significant difference of two groups with statistical significance set at p-values of < 0.05. One-way ANOVA with Tukey post-hoc criterion was used to assess the significance across more than 2 groups.

Results and Discussion

Microstructural Characterization of Dynamic Topography

Strain-induced feature formation is a convenient strategy for rapid programmable presentation of topographic cues. Ordered buckling is an energy-relief mechanism that occurs when a thin rigid membrane on an elastomeric substrate is compressed [39,40]. Releasing the pre-strain of bi-layer substrates produces grating arrays composed of ridge-groove features with short-range order (Figure 3) [41]. This phenomenon has been used as a non-conventional microfabrication technique [42]. Rigid silicon oxide (SiO_2) membranes on polydimethylsiloxane (PDMS) substrates are commonly fabricated by exposing PDMS to O_2 plasma [43,44]. PDMS-SiO_2 bilayers fabricated in this manner typically require large uniaxial strains ($\varepsilon > 10\%$) to create grating arrays [43,45]. One possible explanation is that the minimum thickness of SiO_2 membranes processed using O_2 plasma is large because a significant depth of the PDMS must be converted into SiO_2 before a strain-sensitive percolating network of oxide structures is formed within the substrate. The alternative method described herein uses thermal evaporation of SiO to deposit homogeneous SiO_x (with $1.5 < x < 2$) film apical to PDMS substrates [46]. This approach reduces the effective critical strain required for feature formation via compression. Although the exact composition of SiO_x rigid membranes depends upon the deposition procedure, the composition will hereby be referred to as SiO_2 for simplification.

The morphologies of PDMS-SiO_2 bilayers in flat (F) and wavy ($W_\perp$) configurations are shown in Figure 2. Cycling the strain forms microstructures reversibly as indicated by optical and scanning probe microscopy. AFM images of bilayers in flat configuration ($\varepsilon = 0\%$) contain features with characteristic peak-to-trough amplitudes of approximately 2 nm. This feature height is an order of magnitude smaller than the minimum detection limit for mammalian cells [20,47]. The size of the microstructure of the grating is a strong function of the intensive mechanical properties of the two materials: the thickness of the membrane h_f, and the amount of pre-strain ε_{pre} [48,49]. The anticipated values for average peak-to-through amplitude A_0 and wavelength of the features λ_0 in grating arrays with net compressive strains can be predicted using the following relationships:

$$\lambda_0 = 2\pi h_f \left(\frac{E_f}{3E_s}\right)^{1/3} \quad \text{Eqn. 2}$$

$$A_0 = h_f\sqrt{\frac{\varepsilon_{pre}}{\varepsilon_c} - 1} \quad \text{Eqn. 3}$$

The parameters in each equation are as follows: h_f is the thickness of the rigid membrane; E_f and E_s are Young's moduli of substrate and rigid membrane, respectively; ε_{pre} is amount of uniaxial pre-strain; ε_c is critical buckling strain given by [49]:

$$\varepsilon_c = \frac{1}{4}\left(\frac{3E_s}{E_f}\right)^{2/3} \quad \text{Eqn. 4}$$

A buckling pattern is established only when the applied strain exceeds ε_c. Values for λ_0 are predicted to be largely independent of the amount of pre-strain. However, experimentally observed values of λ_0 are reduced for uniaxial strains greater than 10% [49–51]. Relationships that describe feature sized formed via spontaneous buckling are valid if certain criteria are satisfied. The intensive properties and extensive geometry of the film must be such that $E_f \gg E_f$ and $h_f \ll t_s$ where t_s is the substrate thickness. The net strain $\Delta\varepsilon$ is defined as the difference between the resulting applied strain ε_{app} and the pre-strain via $\Delta\varepsilon = \varepsilon_{app} - \varepsilon_{pre}$. Feature formation either by compression or tension ($|\varepsilon_{app}| > \varepsilon_{pre}$) yields grating features with peak-to-trough amplitudes of $A > 400$ nm. Topographic features produced from pre-strained PDMS-SiO_2 bilayer substrates in this study were consistent with constitutive relationships in Eqns. 2—4. Releasing the pre-strain produces a net compressive strain $\varepsilon_{app} < \varepsilon_{pre}$ and a uniaxial grating array that is oriented orthogonally to the axis of the applied strain. Orthogonal features have an average amplitude of $A_\perp = 429.3 \pm 5.8$ nm and $\lambda_\perp = 4.95 \pm 0.36$ μm (Figure 2). Applying a strain ε_{app} such that $\Delta\varepsilon = 0\%$ abolishes the grating. Tensile strains of $\Delta\varepsilon = \varepsilon_{app} - \varepsilon_{pre} > 3\%$ produce grating arrays parallel to the axis of applied strain. Parallel features have an average amplitude of $A_\parallel = 483.6 \pm 7.8$ nm and $\lambda_\parallel = 4.78 \pm 0.16$ μm. Features emerge for strains as small as $\Delta\varepsilon = |\varepsilon_{app} - \varepsilon_{pre}| = 3\%$. Fast Fourier Transforms (FFT) of optical micrographs are shown in Figure 3b. The intensity and orientation of these data confirm the presence (absence) and orientation of grating arrays under compression, tension, and zero-strain states. The feature amplitude A is also a strong function of the SiO_2 membrane thickness h_f. Optical and scanning probe micrographs of PDMS-SiO_2 bilayer substrates with $h_f = 10$ nm, pre-strain of $\varepsilon_{pre} = +3\%$, and an applied strain of $\Delta\varepsilon = -3\%$ produce random isotropic features with no short-range order and an Rms roughness of 0.317 ± 0.048 nm (Figure 2). Strain-dependent topography can be cycled without any observed hysteresis in feature size. "Strain cycles could likely be repeated dozens of times without any fatigue or fracture of the SiO_2 membrane or mechanical failure of the PDMS substrate." PDMS-SiO_2 bilayer substrates formed by thermal evaporation of SiO_2 membranes offer additional advantages for use in dynamic presentation of substrate topography. First, the minimum critical strain ε_c is reduced, which minimizes crosstalk from mechanical stimuli during quantification of cytoskeleton remodeling [52]. Second, small strains can alter the surface topography between three discrete states: flat (F), orthogonal wavy ($W_\perp$), and parallel wavy ($W_\parallel$). The precise selection of the SiO_2 membrane permits

facile fabrication of control substrates that are identical to dynamic topography substrates in terms of surface chemistry and applied strain. Lastly, topography can be presented both rapidly (~5 sec) and reversibly without indirectly impacting feature geometry.

Morphological Responses of Fibroblasts to Static Topography

FB cultured on static flat (Static F) exhibit a more rounded morphology and random spreading compared to the aligned morphologies of fibroblasts cultured on static grating arrays (Wavy W) as assessed by fluorescent microscopy (Figure 4). Four parameters were used to quantify FB morphology: circularity C_{cell}, ratio of major-to-minor axes R_{axis}, projected area A_{proj}, and angle of major axis to grating direction θ_{align} [37,53]. FB cultured on flat substrates exhibit a larger average cell circularity (0.30 ± 0.13 versus 0.15 ± 0.08; $p<0.001$) and a higher average angle between the major axis of the cell and the features compared to topographic substrates (43.25° ± 23.40° versus 15.22° ± 13.10°; *** $p<0.001$) (Figure 5). These results suggest that static surfaces with grating topography can recapitulate the highly conserved morphological response of mammalian cells to grating features that is associated with contact guidance [54]. These measurements produce a baseline to compare the evolution of FB cytoskeleton morphology on substrates with dynamic topography.

Cell Culture on Substrates with Programmable Topography

Many mammalian cell phenotypes respond to dynamic topographical features through cytoskeleton reorganization [26]. The strain detection threshold for mammalian cells in response to uniaxial stretching is $\varepsilon_{cycle} = 3.5\%$ as inferred by gross morphological characterization [35,36]. This threshold provides a benchmark to limit the maximum applies strains to $|\Delta\varepsilon| < 3.5\%$. Nevertheless, applying strain in sub-threshold regimes may still impact other as of yet unknown aspects of cell-materials interactions. Therefore, several substrate topography sequences were utilized to assess the potential impact of strains in the sub-threshold regime. Static substrates that are either Flat (F) or Wavy (W) are mapped to corresponding dynamic substrates with the following sequences: $FW_{\perp}F$ and $FW_{\perp}$. Substrates with $FW_{\perp}F$ sequences are critical control conditions to measure the potential impact of the transient strain on the downstream cytoskeleton morphodynamics. Furthermore, a direct comparison between sequences of $FW_{\perp}F$ and $FW_{\perp}$ can isolate the direct impact of dynamic topography presentation on cytoskeleton morphology. FB morphology was largely preserved immediately after applied strains of $\Delta\varepsilon = \pm 3\%$ (Figure 6). The orthogonal and parallel axes refer to the relative orientation of the grating features to the direction of applied strain. The morphology of FB cultured on PDMS substrates coated with 10 nm SiO_2 membranes was measured for $t \leq 6$ hr (Figure 7). PDMS substrates with SiO_2 membranes of $h_f = 10$ nm, $\varepsilon_{pre} = +3\%$, and $\Delta\varepsilon = -3\%$ exhibit random gratings with feature sizes of $A = 1.53 \pm 0.55$ nm and $\lambda = 1.8 \pm 0.1$ μm. These features do not significantly alter FB morphology via contact guidance mechanisms since the feature heights are smaller than 35 nm, the previously reported detection limit for contact guidance [55]. PDMS substrates with 10 nm SiO_2 membranes serve as valuable control materials since the strain and chemistry of the substrate are identical to PDMS-SiO_2 bilayers that with thicker SiO_2 membranes. Maintaining constant material properties in dynamic substrates can be challenging [5]. Thin film deposition and precise strains achieve dynamic programmable

topography while preserving many of the other physicochemical aspects of the cellular microenvironment.

After 24 hr of cell seeding ($t = 0$ hr), the surface topography is switched either from flat to wavy ($FW_{\perp}$) or flat to wavy to flat ($FW_{\perp}F$) in rapid succession. The dynamic presentation of substrate topography induces alterations in FB morphology that initiate within 6 min and persist for $t > 6$ hr (Figure 7). The circularity and ratio of major/minor axes of the ($FW_{\perp}$) both exhibit a significant change within 5 min of substrate actuation (** $p < 0.01$), while the average projected area A and major axis angle exhibit significant differences within 1 hour (** $p < 0.001$). Substrates with $FW_{\perp}F$ programs present gratings briefly (5 ± 3 sec). FB cultured on $FW_{\perp}F$ programs exhibit cytoskeleton dynamics that are substantially different compared to Static F substrates. $FW_{\perp}F$ sequences induce transient alterations in the following parameters that are associated with elongated morphologies: circularity C_{cell}, projected area A_{proj}, and axial ratio R_{axis}. Values for C_{cell} and R_{axis} in FB populations cultured on substrates with $FW_{\perp}F$ sequences converge to values observed in cells on Static F substrates for $t \leq 2$ hr. These results suggest that sub-threshold strains induce transient fluctuations in morphological response. Temporary presentation of topographical cues may engage memory mechanisms in mammalian cells that have been previously reported in the context of other types of dynamic cell-materials interactions [56].

Substrates with $FW_{\perp}$ sequences yield morphological changes in FB that are internally consistent with other observations within this study. Substrate actuation via compressive strains is comparable between $FW_{\perp}$ and $FW_{\perp}F$ sequences. FB cultured on substrates with $FW_{\perp}$ sequences adopt a temporary rounded morphology that is manifested by a transient decrease in A_{proj} for $t = 1$ hr (*** $p < 0.001$), a decrease in C_{cell} at $t = 0.1$ hr (*** $p < 0.001$), and an increase in R_{axis} at $t = 0.1$ hr (** $p < 0.01$) compared to Static F substrates (Figure 7). The morphology of FB cultured on substrates with $FW_{\perp}$ sequences for $t \geq 6$ hr compared to Static F substrates approximate that of Static W compared to Static F. These results suggest that steady state FB morphology is achieved within 6 hr.

Single Cell Sensing on Programmable Substrates

Programmable substrates can measure the cytoskeleton morphology of individual FB to transiently altered strain-induced topography. Isolated FB alter their shape and orientation for $t \leq 1$ hr. Single cell morphological responses observed in FB populations cultured on substrates with $FW_{\perp}$ and $FW_{\perp}F$ sequences are shown in Figure 8. FB alignment and elongation occurs for $t < 2$ hr for $FW_{\perp}$ sequences. FB cultured on substrates with $FW_{\perp}F$ sequences extend lamellipodia in seemingly random directions within $t < 2$ hr. Single-cell morphodynamics are consistent with morphological observations made in FB populations. A notable observation is that both $FW_{\perp}$ and $FW_{\perp}F$ sequences induce an initial temporary phase of cell rounding immediately after substrate actuation. This observation is curious because the minimum apparent strain detection threshold during cyclic stretching is $\varepsilon_{cycle} = 3.5\%$. Furthermore, the strains applied in this system are approximately 1 order of magnitude smaller than other experiments that employ dynamic strain. Typical cyclic strain experiments require uniaxial substrate strains of $\varepsilon_{cycle} > 10\%$ [57]. Furthermore, the impact of mechanical stress on cytoskeleton dynamics typically results in strains of $\gamma \sim 20\%$

[58,59]. It is unlikely that the application of transient strains will directly impact binding between integrins and adhesion-promoting peptides because of the strength of these bonds [60]. Typical dissociation constants for this specific kind of receptor-ligand interaction is on the order of $K_D = 10^{-9}$ M, which corresponds to a characteristic binding distance of $r_0 = 3$ nm [60]. Considering the characteristic dimension of integrins is ~10 nm [61], it is likely that 3% strains will not dissociate integrin-peptide coupling. Dynamic topography presentation may, however, alter other downstream effectors of cell-matrix interactions. Transient substrate strains may disrupt focal adhesions or cytoskeleton proteins that induce an altered state in which the cell rapidly interrogates the local chemical and topographical microenvironments by forming nascent integrins [62]. This topic is the subject of ongoing research.

Conclusions

We describe a lithography-free approach to fabricate dynamic substrate topography for measuring morphodynamics of cells during contact guidance. This substrate is advantageous because it presents ordered topographical cues in a manner that decouples potential contributions from other stimuli including substrate chemistry and large mechanical strains. Homogeneous surface chemistry (SiO_2) and small required extensive strains (~3%) are key features of the approach described herein. Although the substrate cannot completely eliminate the effect of external mechanical stimuli on in vitro cell-topography interactions, using small strains minimizes the impact of the applied stimulus. This work represents a strategy to better isolate the effect of dynamic programmable topography on living cells. Furthermore, this technique permits rapid and reversible presentation of topographic cues with precise temporal precision. Dynamic substrate topography afforded by the strategy described herein could be further applied to studying signal transduction pathways that original from transient cell-matrix interactions and propagate to downstream pathways that control cytoskeleton reorganization. Thus, programmable substrate topography is a promising strategy to elucidate cytoskeleton remodeling dynamics in many cell phenotypes in the context of cell-biomaterials interactions.

Supplementary Material

Refer to Web version on PubMed Central for supplementary material.

Acknowledgments

The authors would like to acknowledge the following people for their help: Stephanie Chang and Prof. Yu-li Wang for providing the NIH 3T3 cells; Patrick Boyer and Prof. Kris Dahl for providing the liquid nitrogen storage tank; Haibing Teng, Margaret Fuhrman, and Alan Waggoner (Director) of MBIC/CMU for use of the facilities and technical assistance. The authors would also like to acknowledge funding provided by the National Institutes of Health (NIBIB R21RB015165).

References

1. Cheng C-M, Steward RL, LeDuc PR. Probing cell structure by controlling the mechanical environment with cell-substrate interactions. J Biomech. 2009; 42:187–92. DOI: 10.1016/j.jbiomech.2008.10.014 [PubMed: 19064266]

2. Dalby MJ, Riehle MO, Sutherland DS, Agheli H, Curtis ASG. Changes in fibroblast morphology in response to nano-columns produced by colloidal lithography. Biomaterials. 2004; 25:5415–22. [PubMed: 15130726]

3. Davis KA, Burke KA, Mather PT, Henderson JH. Dynamic cell behavior on shape memory polymer substrates. Biomaterials. 2011; 32:2285–93. DOI: 10.1016/j.biomaterials.2010.12.006 [PubMed: 21224032]

4. Guvendiren M, Burdick JA. Engineering synthetic hydrogel microenvironments to instruct stem cells. Curr Opin Biotechnol. 2013; 24:841–6. DOI: 10.1016/j.copbio.2013.03.009 [PubMed: 23545441]

5. Kim J, Hayward RC. Mimicking dynamic in vivo environments with stimuli-responsive materials for cell culture. Trends Biotechnol. 2012; 30:426–39. DOI: 10.1016/j.tibtech.2012.04.003 [PubMed: 22658474]

6. Spivey EC, Khaing ZZ, Shear JB, Schmidt CE. The fundamental role of subcellular topography in peripheral nerve repair therapies. Biomaterials. 2012; 33:4264–76. DOI: 10.1016/j.biomaterials.2012.02.043 [PubMed: 22425024]

7. Nikkhah M, Edalat F, Manoucheri S, Khademhosseini A. Engineering microscale topographies to control the cell–substrate interface. Biomaterials. 2012; 33:5230–46. [PubMed: 22521491]

8. Kim HN, Jiao A, Hwang NS, Kim MS, Kang DH, Kim D-H, et al. Nanotopography-guided tissue engineering and regenerative medicine. Adv Drug Deliv Rev. 2013; 65:536–58. DOI: 10.1016/j.addr.2012.07.014 [PubMed: 22921841]

9. Franco D, Milde F, Klingauf M, Orsenigo F, Dejana E, Poulikakos D, et al. Accelerated endothelial wound healing on microstructured substrates under flow. Biomaterials. 2013; 34:1488–97. DOI: 10.1016/j.biomaterials.2012.10.007 [PubMed: 23182348]

10. Leclerc A, Tremblay D, Hadjiantoniou S, Bukoreshtliev NV, Rogowski JL, Godin M, et al. Three dimensional spatial separation of cells in response to microtopography. Biomaterials. 2013; 34:8097–104. DOI: 10.1016/j.biomaterials.2013.07.047 [PubMed: 23899447]

11. Tzvetkova-Chevolleau T, Stéphanou A, Fuard D, Ohayon J, Schiavone P, Tracqui P. The motility of normal and cancer cells in response to the combined influence of the substrate rigidity and anisotropic microstructure. Biomaterials. 2008; 29:1541–51. DOI: 10.1016/j.biomaterials.2007.12.016 [PubMed: 18191193]

12. Kolind K, Kraft D, Bøggild T, Duch M, Lovmand J, Pedersen FS, et al. Control of proliferation and osteogenic differentiation of human dental-pulp-derived stem cells by distinct surface structures. Acta Biomater. 2014; 10:641–50. DOI: 10.1016/j.actbio.2013.11.006 [PubMed: 24252446]

13. Han L, Mao Z, Wu J, Guo Y, Ren T, Gao C. Unidirectional migration of single smooth muscle cells under the synergetic effects of gradient swelling cue and parallel groove patterns. Colloids Surf B Biointerfaces. 2013; 111C:1–6. DOI: 10.1016/j.colsurfb.2013.05.011

14. Sheets K, Wunsch S, Ng C, Nain AS. Shape-dependent cell migration and focal adhesion organization on suspended and aligned nanofiber scaffolds. Acta Biomater. 2013; 9:7169–77. DOI: 10.1016/j.actbio.2013.03.042 [PubMed: 23567946]

15. Seo CH, Jeong H, Furukawa KS, Suzuki Y, Ushida T. The switching of focal adhesion maturation sites and actin filament activation for MSCs by topography of well-defined micropatterned surfaces. Biomaterials. 2013; 34:1764–71. DOI: 10.1016/j.biomaterials.2012.11.031 [PubMed: 23219606]

16. Ferrari A, Cecchini M, Serresi M, Faraci P, Pisignano D, Beltram F. Neuronal polarity selection by topography-induced focal adhesion control. Biomaterials. 2010; 31:4682–94. DOI: 10.1016/j.biomaterials.2010.02.032 [PubMed: 20304485]

17. Walboomers XF, Monaghan W, Curtis AS, Jansen JA. Attachment of fibroblasts on smooth and microgrooved polystyrene. J Biomed Mater Res. 1999; 46:212–20. DOI: 10.1002/(SICI)1097-4636(199908)46:2<212::AID-JBM10>3.0.CO;2-Y [PubMed: 10379999]

18. Koo S, Muhammad R, Peh GSL, Mehta JS, Yim EKF. Micro- and nanotopography with extracellular matrix coating modulate human corneal endothelial cell behavior. Acta Biomater. 2014; 10:1975–84. DOI: 10.1016/j.actbio.2014.01.015 [PubMed: 24456758]

19. Zhao G, Raines AL, Wieland M, Schwartz Z, Boyan BD. Requirement for both micron- and submicron scale structure for synergistic responses of osteoblasts to substrate surface energy and

topography. Biomaterials. 2007; 28:2821–9. DOI: 10.1016/j.biomaterials.2007.02.024 [PubMed: 17368532]

20. Biela SA, Su Y, Spatz JP, Kemkemer R. Different sensitivity of human endothelial cells, smooth muscle cells and fibroblasts to topography in the nano-micro range. Acta Biomater. 2009; 5:2460–6. DOI: 10.1016/j.actbio.2009.04.003 [PubMed: 19410529]
21. Flemming RG, Murphy CJ, Abrams GA, Goodman SL, Nealey PF. Effects of synthetic micro- and nano-structured surfaces on cell behavior. Biomaterials. 1999; 20:573–88. [PubMed: 10213360]
22. Lü D, Luo C, Zhang C, Li Z, Long M. Differential regulation of morphology and stemness of mouse embryonic stem cells by substrate stiffness and topography. Biomaterials. 2014; 35:3945–55. DOI: 10.1016/j.biomaterials.2014.01.066 [PubMed: 24529627]
23. Davidson P, Bigerelle M, Bounichane B, Giazzon M, Anselme K. Definition of a simple statistical parameter for the quantification of orientation in two dimensions: application to cells on grooves of nanometric depths. Acta Biomater. 2010; 6:2590–8. DOI: 10.1016/j.actbio.2010.01.038 [PubMed: 20123045]
24. Watari S, Hayashi K, Wood JA, Russell P, Nealey PF, Murphy CJ, et al. Modulation of osteogenic differentiation in hMSCs cells by submicron topographically-patterned ridges and grooves. Biomaterials. 2012; 33:128–36. DOI: 10.1016/j.biomaterials.2011.09.058 [PubMed: 21982295]
25. Chua JS, Chng C-P, Moe AAK, Tann JY, Goh ELK, Chiam K-H, et al. Extending neurites sense the depth of the underlying topography during neuronal differentiation and contact guidance. Biomaterials. 2014; 35:7750–61. DOI: 10.1016/j.biomaterials.2014.06.008 [PubMed: 24954734]
26. Lam MT, Clem WC, Takayama S. Reversible on-demand cell alignment using reconfigurable microtopography. Biomaterials. 2008; 29:1705–12. DOI: 10.1016/j.biomaterials.2007.12.010 [PubMed: 18192004]
27. Yang P, Baker RM, Henderson JH, Mather PT. In vitro wrinkle formation via shape memory dynamically aligns adherent cells. Soft Matter. 2013; 9:4705.doi: 10.1039/c3sm00024a
28. Kloxin AM, Tibbitt MW, Anseth KS. Synthesis of photodegradable hydrogels as dynamically tunable cell culture platforms. Nat Protoc. 2010; 5:1867–87. DOI: 10.1038/nprot.2010.139 [PubMed: 21127482]
29. Straley KS, Heilshorn SC. Dynamic, 3D-Pattern Formation Within Enzyme-Responsive Hydrogels. Adv Mater. 2009; 21:4148–52. DOI: 10.1002/adma.200901865
30. Hui EE, Bhatia SN. Micromechanical control of cell–cell interactions. Proc Natl Acad Sci. 2007; 104:5722–6. DOI: 10.1073/pnas.0608660104 [PubMed: 17389399]
31. Lamb BM, Yousaf MN. Redox-switchable surface for controlling peptide structure. J Am Chem Soc. 2011; 133:8870–3. DOI: 10.1021/ja203198y [PubMed: 21595476]
32. Idota N, Tsukahara T, Sato K, Okano T, Kitamori T. The use of electron beam lithographic graft-polymerization on thermoresponsive polymers for regulating the directionality of cell attachment and detachment. Biomaterials. 2009; 30:2095–101. DOI: 10.1016/j.biomaterials.2008.12.058 [PubMed: 19157534]
33. Wong JY, Leach JB, Brown XQ. Balance of chemistry, topography, and mechanics at the cell–biomaterial interface: Issues and challenges for assessing the role of substrate mechanics on cell response. Surf Sci. 2004; 570:119–33. DOI: 10.1016/j.susc.2004.06.186
34. Kaunas R, Nguyen P, Usami S, Chien S. Cooperative effects of Rho and mechanical stretch on stress fiber organization. Proc Natl Acad Sci U S A. 2005; 102:15895–900. DOI: 10.1073/pnas.0506041102 [PubMed: 16247009]
35. Winston FK, Macarak EJ, Gorfien SF, Thibault LE. A system to reproduce and quantify the biomechanical environment of the cell. J Appl Physiol Bethesda Md 1985. 1989; 67:397–405.
36. Song G, Ju Y, Shen X, Luo Q, Shi Y, Qin J. Mechanical stretch promotes proliferation of rat bone marrow mesenchymal stem cells. Colloids Surf B Biointerfaces. 2007; 58:271–7. DOI: 10.1016/j.colsurfb.2007.04.001 [PubMed: 17499488]
37. Den Braber ET, de Ruijter JE, Ginsel LA, von Recum AF, Jansen JA. Quantitative analysis of fibroblast morphology on microgrooved surfaces with various groove and ridge dimensions. Biomaterials. 1996; 17:2037–44. DOI: 10.1016/0142-9612(96)00032-4 [PubMed: 8902235]

38. Slízová D, Krs O, Pospísilová B. Alternative method of rapid drying vascular specimens for scanning electron microscopy. J Endovasc Ther Off J Int Soc Endovasc Spec. 2003; 10:285–7. DOI: 10.1583/1545-1550(2003)010<0285:AMORDV>2.0.CO;2
39. Bowden N, Brittain S, Evans AG, Hutchinson JW, Whitesides GM. Spontaneous formation of ordered structures in thin films of metals supported on an elastomeric polymer. 1998; 393:146–9. DOI: 10.1038/30193
40. Box F, Bowman R, Mullin T. Dynamic compression of elastic and plastic cellular solids. Appl Phys Lett. 2013; 103:151909.doi: 10.1063/1.4824845
41. Wu H, Kustra S, Gates EM, Bettinger CJ. Topographic substrates as strain relief features in stretchable organic thin film transistors. Org Electron. 2013; 14:1636–42. DOI: 10.1016/j.orgel.2013.02.037
42. Quero, JM., Perdigones, F., Aracil, C. Smart Sensors and Mems. Elsevier; 2014.
43. Yu C, Jiang H. Forming wrinkled stiff films on polymeric substrates at room temperature for stretchable interconnects applications. Thin Solid Films. 2010; 519:818–22. DOI: 10.1016/j.tsf.2010.08.106
44. Béfahy S, Lipnik P, Pardoen T, Nascimento C, Patris B, Bertrand P, et al. Thickness and elastic modulus of plasma treated PDMS silica-like surface layer. Langmuir ACS J Surf Colloids. 2010; 26:3372–5. DOI: 10.1021/la903154y
45. Shih T-K, Ho J-R, Liao H-Y, Chen C-F, Liu C-Y. Fabrication of optical gratings by shrinkage of a rubber material. Thin Solid Films. 2008; 516:5339–43. DOI: 10.1016/j.tsf.2007.07.092
46. Barranco A, Yubero F, Espinós JP, Groening P, González-Elipe AR. Electronic state characterization of SiOx thin films prepared by evaporation. J Appl Phys. 2005; 97:113714.doi: 10.1063/1.1927278
47. Dalby MJ, Riehle MO, Johnstone H, Affrossman S, Curtis ASG. Investigating the limits of filopodial sensing: a brief report using SEM to image the interaction between 10 nm high nano-topography and fibroblast filopodia. Cell Biol Int. 2004; 28:229–36. DOI: 10.1016/j.cellbi.2003.12.004 [PubMed: 14984750]
48. Ohzono T, Monobe H. Microwrinkles: shape-tunability and applications. J Colloid Interface Sci. 2012; 368:1–8. DOI: 10.1016/j.jcis.2011.11.075 [PubMed: 22196350]
49. Jiang H, Khang D-Y, Song J, Sun Y, Huang Y, Rogers JA. Finite deformation mechanics in buckled thin films on compliant supports. Proc Natl Acad Sci U S A. 2007; 104:15607–12. DOI: 10.1073/pnas.0702927104 [PubMed: 17898178]
50. Song J, Jiang H, Huang Y, Rogers JA. Mechanics of stretchable inorganic electronic materials. J Vac Sci Technol A. 2009; 27:1107–25. DOI: 10.1116/1.3168555
51. Harrison C, Stafford CM, Zhang W, Karim A. Sinusoidal phase grating created by a tunably buckled surface. Appl Phys Lett. 2004; 85:4016–8. DOI: 10.1063/1.1809281
52. Houtchens GR, Foster MD, Desai TA, Morgan EF, Wong JY. Combined effects of microtopography and cyclic strain on vascular smooth muscle cell orientation. J Biomech. 2008; 41:762–9. DOI: 10.1016/j.jbiomech.2007.11.027 [PubMed: 18222460]
53. Hakkinen KM, Harunaga JS, Doyle AD, Yamada KM. Direct comparisons of the morphology, migration, cell adhesions, and actin cytoskeleton of fibroblasts in four different three-dimensional extracellular matrices. Tissue Eng Part A. 2011; 17:713–24. DOI: 10.1089/ten.TEA.2010.0273 [PubMed: 20929283]
54. Van Delft FCMJM, van den Heuvel FC, Loesberg WA, te Riet J, Schön P, Figdor CG, et al. Manufacturing substrate nano-grooves for studying cell alignment and adhesion. Microelectron Eng. 2008; 85:1362–6. DOI: 10.1016/j.mee.2008.01.028
55. Dalby MJ, Riehle MO, Johnstone HJH, Affrossman S, Curtis ASG. Polymer-Demixed Nanotopography: Control of Fibroblast Spreading and Proliferation. Tissue Eng. 2002; 8:1099–108. DOI: 10.1089/107632702320934191 [PubMed: 12542955]
56. Yang C, Tibbitt MW, Basta L, Anseth KS. Mechanical memory and dosing influence stem cell fate. Nat Mater. 2014; 13:645–52. DOI: 10.1038/nmat3889 [PubMed: 24633344]
57. Morioka M, Parameswaran H, Naruse K, Kondo M, Sokabe M, Hasegawa Y, et al. Microtubule Dynamics Regulate Cyclic Stretch-Induced Cell Alignment in Human Airway Smooth Muscle Cells. PLoS ONE. 2011; 6:e26384.doi: 10.1371/journal.pone.0026384 [PubMed: 22022610]

58. Zhu X, Mills KL, Peters PR, Bahng JH, Liu EH, Shim J, et al. Fabrication of reconfigurable protein matrices by cracking. Nat Mater. 2005; 4:403–6. DOI: 10.1038/nmat1365 [PubMed: 15834415]

59. Ehrlicher AJ, Nakamura F, Hartwig JH, Weitz DA, Stossel TP. Mechanical strain in actin networks regulates FilGAP and integrin binding to filamin A. Nature. 2011; 478:260–3. DOI: 10.1038/nature10430 [PubMed: 21926999]

60. Lauffenburger, DA. Receptors: Models for Binding, Trafficking, and Signaling. New York: Oxford University Press; 1996.

61. Comisar WA, Mooney DJ, Linderman JJ. Integrin Organization: Linking Adhesion Ligand Nanopatterns with Altered Cell Responses. J Theor Biol. 2011; 274:120–30. DOI: 10.1016/j.jtbi.2011.01.007 [PubMed: 21255586]

62. Beningo KA, Dembo M, Kaverina I, Small JV, Wang Y. Nascent Focal Adhesions Are Responsible for the Generation of Strong Propulsive Forces in Migrating Fibroblasts. J Cell Biol. 2001; 153:881–8. DOI: 10.1083/jcb.153.4.881 [PubMed: 11352946]

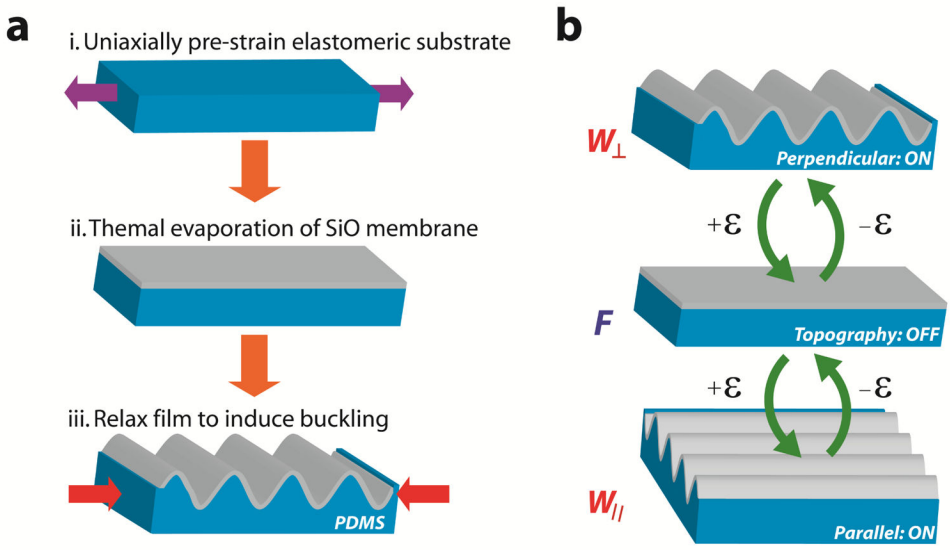

Figure 1.

Fabrication scheme and actuation of reconfigurable dynamic topography. a) The fabrication flow is shown: (i) PDMS substrates are strained to a prescribed amount and (ii) SiO_2 membranes are deposited on the surface using thermal evaporation. (iii) The pre-strain is released to create wavy grating arrays via spontaneous buckling. b) Programmable topography consists of three discrete strain-dependent states that depend on the difference between the pre-strain and applied strain Δε: Δε < 0% produces perpendicular wavy gratings ($W_\perp$); Δε = 0% produces flat substrates (F); Δε > 0% produces parallel wavy gratings ($W_{||}$). These states are shown sequentially from top to bottom as the value of Δε becomes more positive.

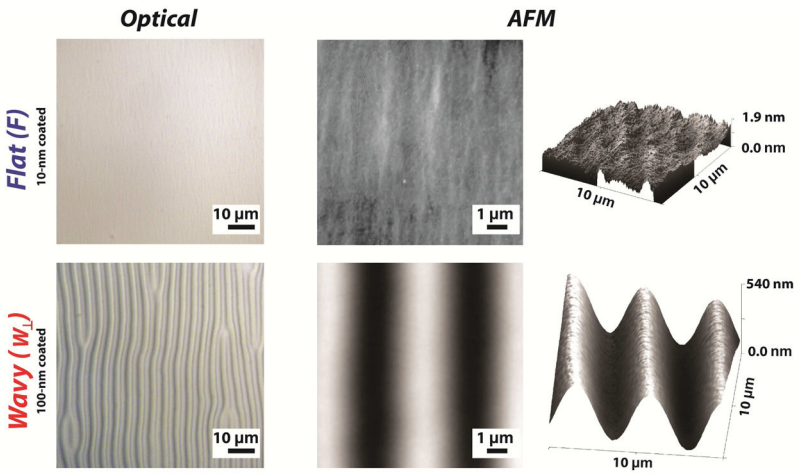

Figure 2.

PDMS coupons are pre-strained to ε_{pre} = +3% and SiO_2 membranes of thickness h_f are deposited on elastomeric substrates. The pre-strain is released such that $\Delta\varepsilon$ = -3% prior to characterization. SiO_2 membranes with h_f = 100 nm generate flat (*F*) surfaces, while SiO_2 membranes with h_f = 100 nm generate substrates with perpendicular gratings ($W_\perp$).

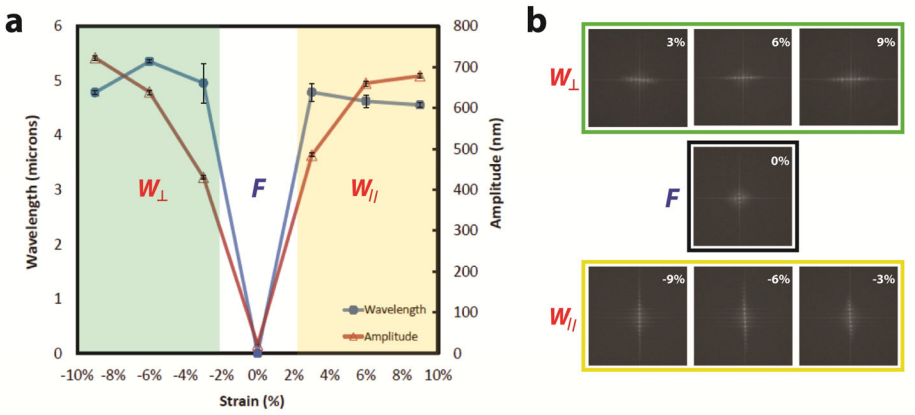

Figure 3.

PDMS-SiO_2 bilayer substrates produce reconfigurable programmable topography. PDMS-SiO_2 bilayer substrates are pre-strained to ε_{pre} = 9% and coated with SiO_2 layers of h_f = 100 nm. a) Wavelengths and amplitudes of the surface features are measured as a function of $\Delta\varepsilon = \varepsilon_{app} - \varepsilon_{re}$. Values of $\Delta\varepsilon < 0\%$, $\Delta\varepsilon = 0\%$ and $\Delta\varepsilon > 0\%$ generate perpendicular wavy gratings ($W_\perp$), featureless flat substrates (F), and parallel wavy gratings ($W_{||}$)features, respectively. b) Fast Fourier Transforms (FFT) of PDMS-SiO_2 bilayer substrates with the for $-9\% < \Delta\varepsilon < +9\%$. The intensity and relative orientation of FFT signals confirm the presence (absence) of distinguishable features and the orientation of wavy grating arrays in the following discrete states: $W_\perp$, F, and $W_{||}$.

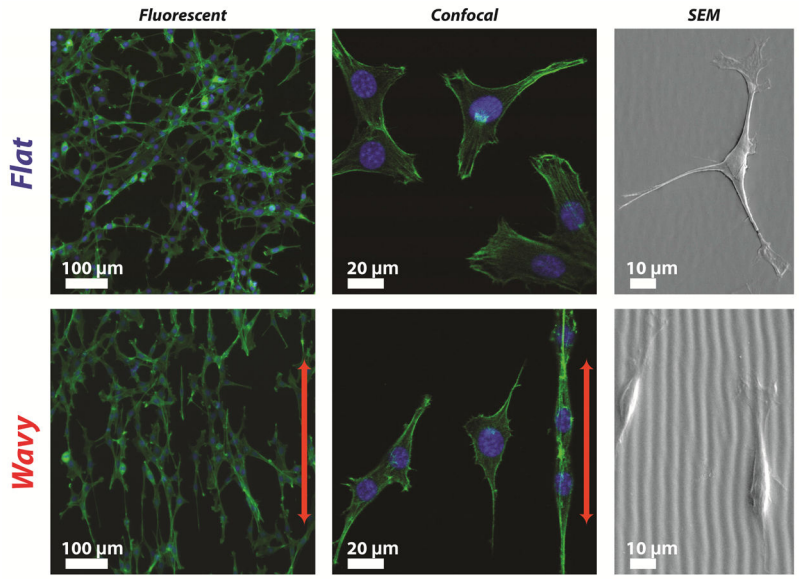

Figure 4.

Fibroblast morphology and orientation on static flat (*F*) and static wavy gratings (*W*). Fibroblasts are fixed on PDMS-SiO_2 bilayers for 24 hr prior to characterization. Micrographs suggest that fibroblasts were randomly oriented on static flat (*F*) substrates and aligned to wavy gratings (*W*). The direction of the grating is indicated by the red arrows. Actin and nuclei are shown in green and blue, respectively.

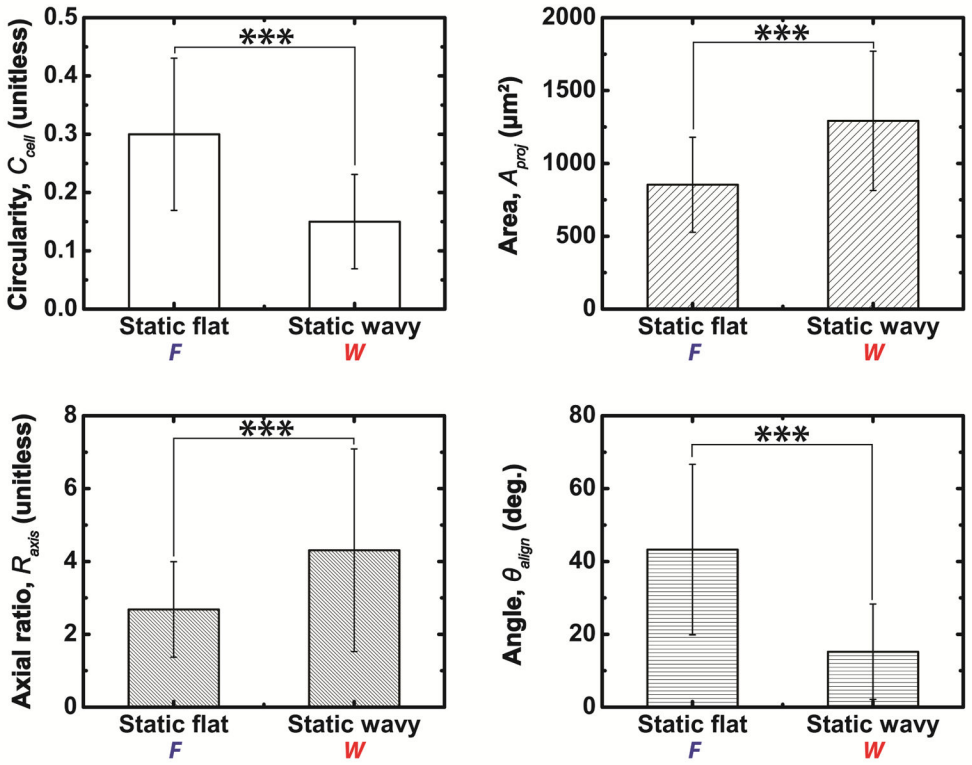

Figure 5.

Quantification of fibroblast morphology and orientation on substrates with static flat (*F*) and static perpendicular gratings ($W_{\perp}$). Values of circularity C_{cell}, projected area A_{proj}, axial ratio R_{axis}, and alignment angle θ_{align} confirm that fibroblasts exhibit reduced spreading and increased alignment and orientation when cultured on $W_{\perp}$ substrates compared to *F* substrates (*** $p<0.001$).

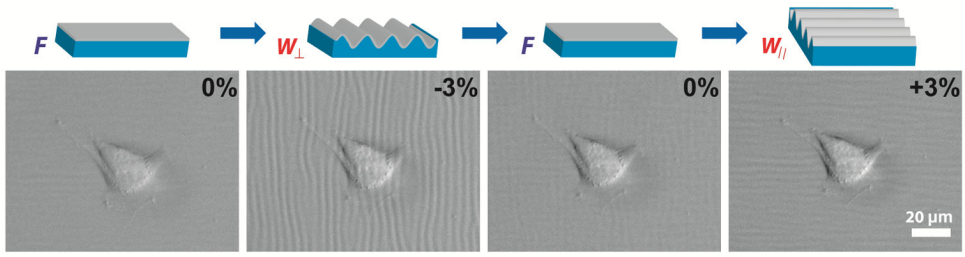

Figure 6.

Transient response of isolated fibroblast in response to PDMS-SiO_2 bilayers cycled through discrete states of substrate topography. The applied strain is applied rapidly to achieve the following configurations: The strain is sequentially and quickly applied across the following values: $\Delta\varepsilon = 0\%$ generates flat substrates (F) with no grating features; $\Delta\varepsilon = +3\%$ produces perpendicular wavy grating arrays ($W_{\perp}$); $\Delta\varepsilon = -3\%$ produces wavy grating arrays that are parallel to the axis of applied strain ($W_{\parallel}$). The rapid switching of substrate topographies does not induce observable morphological changes in FB over the span of 30 sec.

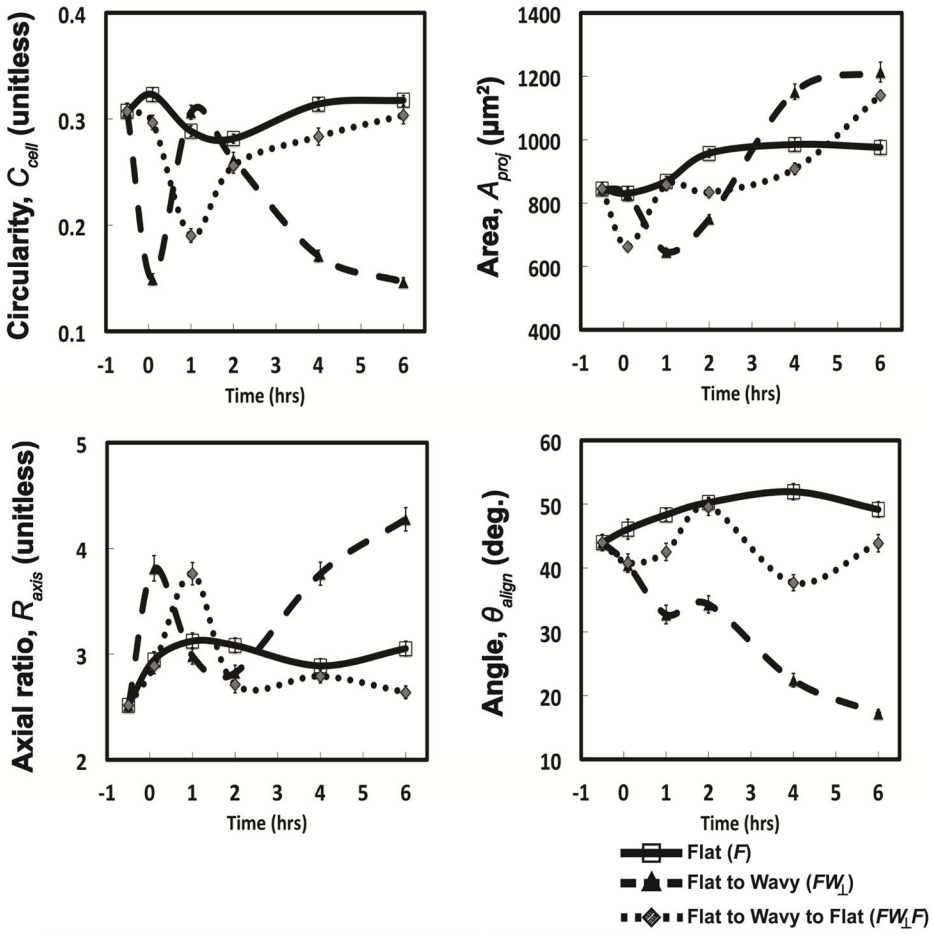

Circularity	0.1h	1h	2h	4h	6h
F vs. $FW_{\perp}$	***	-	-	***	***
F vs. $FW_{\perp}F$	-	***	-	-	-
$FW_{\perp}$ vs. $FW_{\perp}F$	***	***	-	***	***

Area	0.1h	1h	2h	4h	6h
F vs. $FW_{\perp}$	-	***	***	**	***
F vs. $FW_{\perp}F$	***	-	**	-	***
$FW_{\perp}$ vs. $FW_{\perp}F$	***	***	*	***	-

Axial ratio	0.1h	1h	2h	4h	6h
F vs. $FW_{\perp}$	**	-	-	***	***
F vs. $FW_{\perp}F$	-	**	-	-	-
$FW_{\perp}$ vs. $FW_{\perp}F$	***	**	-	***	***

Angle	0.1h	1h	2h	4h	6h
F vs. $FW_{\perp}$	-	***	***	***	***
F vs. $FW_{\perp}F$	-	-	-	***	-
$FW_{\perp}$ vs. $FW_{\perp}F$	-	**	***	***	***

Figure 7.

Cytoskeleton morphodynamics for FB cultured on substrates over the course of 6 hr with the following sequences are shown: Static flat (*F*), dynamic flat to wavy grating ($FW_{\perp}$), and dynamic flat to wavy grating back to flat ($FW_{\perp}F$). Results of one-way ANOVA with Tukey post hoc tests are summarized in the table.

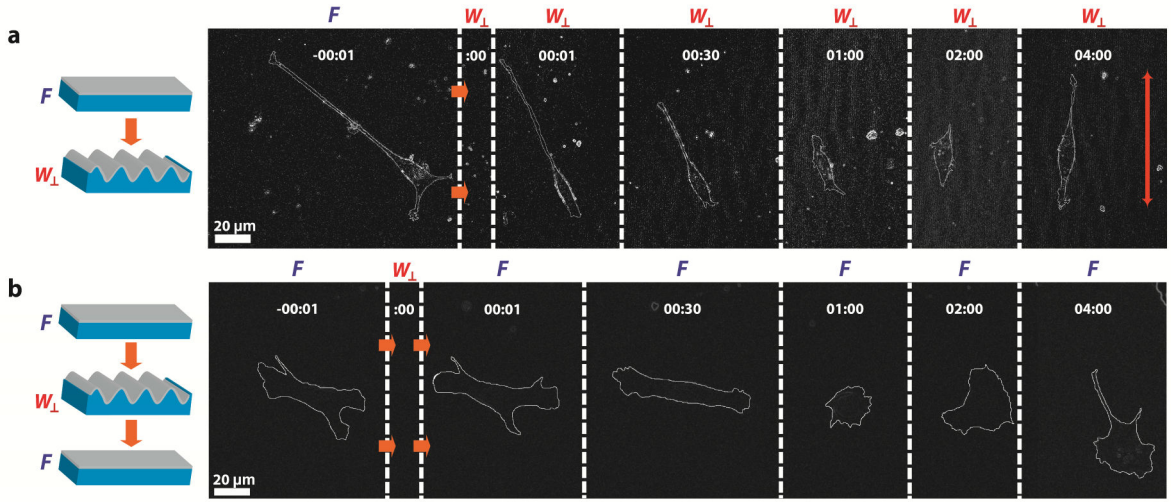

Figure 8.

Morphodynamics of a single FB in response to substrate perturbations. Single cells are captured before and after topographical switching, indicated at zero time point (:00). Phase contrast micrographs are processed using ImageJ to depict changes of cellular shape and orientation. Substrates are programmed with the following sequences: (a) flat to perpendicular wavy grating ($FW_{\perp}$); (b) flat to perpendicular wavy grating back to flat substrates ($FW_{\perp}F$).